Hindawi
Journal of Mathematics
Volume 2023, Article ID 8723343, 10 pages
https://doi.org/10.1155/2023/8723343

Research Article

Vieta-Lucas Collocation Technique for Examination of the Flow of Casson Fluid over a Slippery Stretching Sheet Which Is Impacted by Thermal Slip, Ohmic Dissipation, and Variable Thermal Conductivity

A. Eid,[1,2] **M. M. Khader**,[3,4] **and Ahmed M. Megahed**[4]

[1]*Department of Physics, College of Science, Imam Mohammad Ibn Saud Islamic University (IMSIU), Riyadh 11566, Saudi Arabia*
[2]*Department of Physics, Faculty of Science, Cairo University, Giza, Egypt*
[3]*Department of Mathematics and Statistics, College of Science, Imam Mohammad Ibn Saud Islamic University (IMSIU), Riyadh 11566, Saudi Arabia*
[4]*Department of Mathematics, Faculty of Science, Benha University, Benha, Egypt*

Correspondence should be addressed to A. Eid; amaid@imamu.edu.sa

Received 1 December 2022; Revised 15 January 2023; Accepted 5 April 2023; Published 25 April 2023

Academic Editor: M. M. Bhatti

This work aimed to present the influence of the magnetic field and Ohmic dissipation on the non-Newtonian Casson fluid on a vertical stretched sheet to numerically solve the problem. Here, the variable thermal conductivity is taken as a linear function of temperature. Electric fields, thermal slip, and viscous dissipation effects are taken into consideration. A collection of physical conditions on the sheet's enclosing wall and the momentum and heat transport processes are expressed as partial differential equations (PDEs). Some of the similarity transformations are used to convert the collection of PDE into a system of ordinary differential equations. This system is numerically treated by implementing the Vieta-Lucas spectral collocation method. Some observations are made for the investigation of method convergence. The effect of some different parameters on the velocity and temperature profiles is graphically represented. Additionally, this area of study has significant practical applications in a variety of industries, including paper production, thermal power generation, nuclear reactors, cooling of metallic sheets, glass fiber, and lubrication.

1. Introduction

The flow of non-Newtonian fluids (n-NFs) has gained a great deal of interest in recent decades because it has a wide range of important technological applications. This type of fluid has many uses in industrial applications, including the widespread use of molten plastics, blood, slurries, and paints. Non-Newtonian fluids respond to stress in different ways: some grow more solid and some become more fluid. Depending on the amount of tension applied or the length of time the stress is applied, the properties of non-Newtonian fluids may alter. These n-NFs are divided into distinct classes based on their different properties. As a result, the expanding kinds of n-NFs have recently aroused the curiosity of researchers. The n-NFs models of many distinct types have been studied, including the power-law model [1], the viscoelastic model [2], the Carreau model [3], the Maxwell model [4], the Williamson model [5], the micropolar model [6, 7], the Powell-Eyring model [8], and the Sisko model [9].

The Casson model class, which combines shear-thinning with shear-thickening, is the most popular of the aforementioned non-Newtonian models. If the fluid's shear stress does not exceed its yield stress, the Casson fluid model behaves similar to a solid. Researchers became particularly intrigued by Casson fluids because of their uses in the manufacture of biological fluids, pigments, and China clay [10]. There are a number of intriguing articles pertaining to the Casson fluid flow model [11–13]. Due to their many applications in fluid mechanics, biology, viscoelasticity, engineering, and physics, ordinary and PDEs have been the subject of many

investigations. As a result, the solutions of ordinary differential equations (ODEs) of physical relevance have received a lot of attention. We used the Vieta–Lucas spectral collocation method (SCM) to solve the nonlinear ODEs that regulate the physical problem quantitatively.

Having carefully read the aforementioned works and to the best of our knowledge, for the non-Newtonian Casson fluid flow with viscous dissipation and slip velocity, no attempt has been made to obtain the numerical solutions by using the Vieta–Lucas spectral collocation method. Due to this, the goal of this research is to investigate the approximate solutions for the model under study by implementing the SCM based on the shifted Vieta–Lucas polynomials (VLPs) [14]. The most famous advantage of these methods is their capability to generate accurate outcomes with a very small degree error of freedom [14]. The orthogonality property of the shifted Vieta–Lucas polynomials is used to approximate functions on its domain. These polynomials have a main and important role in these methods for ODEs [15]. Many researchers used and implemented these polynomials to solve numerically many problems, such as in [16], they were used to solve the nonlinear generalized Benjamin–Bona–Mahony–Burgers equation, and in [17], they were used to solve the sinh–Gordon equation. The study's novelty and purpose stem from the fact that it is the first of its type to implement the proposed numerical technique to solve the proposed model.

2. Mathematical Modeling of the Problem

We considered the flow of a non-Newtonian Casson fluid across the vertical rough stretching sheet that is electrically conducting, steady, and incompressible. In the energy equation relationship, the Ohmic dissipation, and viscous dissipation properties are taken into account. The motion of the Casson fluid is produced by velocity $U_w = ax$. The elastic sheet's plane is the x-axis selection, and the plane's normal to it is the y-axis as depicted in Figure 1. In this study, we assumed that the fluid flow is constrained by the presence of magnetic field of strength B_0, whereas the fluid temperature is affected by the viscous dissipation phenomenon. Where u and v are the velocity components in the x and y directions, respectively. Likewise, the density of the Casson fluid is symbolized by ρ. The controlling nonlinear expressions are as follows under the aforementioned assumptions [18, 19]:

$$\frac{\partial u}{\partial x} + \frac{\partial v}{\partial y} = 0, \tag{1}$$

$$u\frac{\partial u}{\partial x} + v\frac{\partial u}{\partial y} = \nu\left(1 + \frac{1}{\beta}\right)\frac{\partial^2 u}{\partial y^2} + \frac{\sigma}{\rho}\left(E_0 B_0 - B_0^2 u\right) + g\delta\left(T - T_\infty\right), \tag{2}$$

$$u\frac{\partial T}{\partial x} + v\frac{\partial T}{\partial y} = \frac{1}{\rho c_p}\frac{\partial}{\partial y}\left(\kappa\frac{\partial T}{\partial y}\right) + \frac{\sigma}{\rho c_p}\left(uB_0 - E_0\right)^2 + \frac{\mu}{\rho c_p}\left(1 + \frac{1}{\beta}\right)\left(\frac{\partial u}{\partial y}\right)^2, \tag{3}$$

where $\beta, \mu, \kappa, \sigma, B_0, T, c_p, \nu, g,$ and δ are, respectively, the Casson parameter, fluid viscosity, thermal conductivity, electrical conductivity of fluid, magnetic field strength, temperature of fluid, specific heat, kinematic viscosity, gravitational acceleration, and the coefficient of thermal expansion. The subjected boundary constraints are as follows [20]:

$$\begin{aligned} u &= U_w + \lambda_1\left(1 + \frac{1}{\beta}\right)\frac{\partial u}{\partial y}, \\ v &= 0, \\ T &= T_w + K\frac{\partial T}{\partial y}, \\ &\text{at } y = 0, \end{aligned} \tag{4}$$

$$u \longrightarrow 0,\ T \longrightarrow T_\infty, \text{as } y \longrightarrow \infty. \tag{5}$$

Here, it is crucial to highlight that this study considers the slip velocity phenomenon, as shown by the first portion of equation (4), whereas the sheet is impermeable according to the second portion of the same equation, where K denotes the thermal slip coefficient and λ_1 denotes the slip velocity coefficient, both of which have the dimension m. The dimensionless of velocity and temperature exists if we introduce the following transformations [21]:

$$\begin{aligned} \eta &= \left(\frac{a}{\nu}\right)^{1/2} y, \\ u &= axf'(\eta), \\ v &= -(a\nu)^{1/2} f(\eta), \end{aligned} \tag{6}$$

$$\theta(\eta) = \frac{T - T_\infty}{T_w - T_\infty}, \tag{7}$$

where θ is the dimensionless temperature and f' is the dimensionless velocity. Furthermore, the accurate estimation of the heat transfer mechanism can be achieved for the assumption of fluid variable thermal conductivity. Therefore, here, the thermal conductivity κ is assumed to obey the following relation [22]:

$$\kappa = \kappa_\infty(1 + \varepsilon\theta(\eta)), \tag{8}$$

where ε is the thermal conductivity parameter and κ_∞ is the ambient thermal conductivity. Evidently, equation (6) already meets the continuity equation (1). Utilizing the previously stated relations (6) and (7) leads to the following governing equations:

$$\left(1 + \frac{1}{\beta}\right)f''' + ff'' - f'^2 + M^2\left(E_1 - f'\right) + \Delta\theta = 0, \tag{9}$$

$$\frac{1}{\mathrm{Pr}}\left((1 + \varepsilon\theta)\theta'' + \varepsilon\theta'^2\right) + M^2 Ec\left(f' - E_1\right)^2 + f\theta' + Ec\left(1 + \frac{1}{\beta}\right)f''^2 = 0, \tag{10}$$

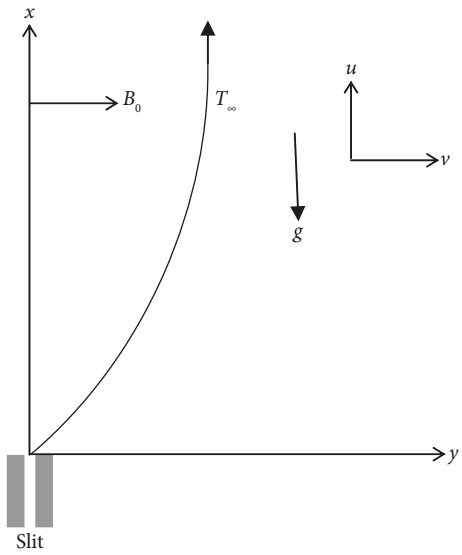

Figure 1: Schematic diagram of the model.

with the following applicable boundary constraints:

$$f(0) = 0,$$

$$f'(0) = 1 + \lambda\left(1 + \frac{1}{\beta}\right)f''(0), \tag{11}$$

$$\theta(0) = 1 + S_T\theta',$$

$$f'(\eta) \longrightarrow 0, \theta(\eta) \longrightarrow 0, \text{as } \eta \longrightarrow \infty, \tag{12}$$

where the mixed convection parameter, slip velocity parameter, local electric parameter, magnetic parameter, thermal slip parameter, Prandtl number, Eckert number are defined, respectively, as follows:

$$\begin{aligned} \Delta &= \frac{g\delta}{a(T_w - T_\infty)}, \\ \lambda &= \lambda_1\sqrt{\frac{a}{\nu}}, \\ E_1 &= \frac{E_0}{aB_0x}, \\ M^2 &= \frac{\sigma B_0^2}{\rho a}, \end{aligned} \tag{13}$$

$$\begin{aligned} S_T &= K\sqrt{\frac{a}{\nu}}, \\ \Pr &= \frac{\mu c_p}{\kappa_\infty}, \\ Ec &= \frac{U_w^2}{c_p(T_w - T_\infty)}. \end{aligned} \tag{14}$$

The importance physical quantities in this study are the skin friction coefficient and the local Nusselt number which is given by the following equation:

$$\begin{aligned} C_f Re_x^{1/2} &= -\left(1 + \frac{1}{\beta}\right)f''(0), \\ Nu_x Re_x^{-1/2} &= -(1 + \varepsilon)\theta'(0), \end{aligned} \tag{15}$$

where $Re_x = U_w x/\nu$ is the local Reynolds number.

3. Procedure of Solution

3.1. Approximate the Solution. In this subsection, we give some definitions and properties of the shifted VLPs to solve the problem under study in $[0, \hbar]$. We used the transformation $z = (4/\hbar)\eta - 2$ to generate a new orthogonal family of the VLPs on $[0, \hbar]$ and so-called the shifted VLPs which is denoted by $\mathrm{VL}_k^s(\eta)$ and may be given as follows [23, 24]:

$$\mathrm{VL}_k^s(\eta) = \mathrm{VL}_k\left(\left(\frac{4}{\hbar}\right)\eta - 2\right). \tag{16}$$

The polynomials $\mathrm{VL}_k^s(\eta)$ yield from the following recurrence relation:

$$\begin{aligned} \mathrm{VL}_{k+1}^s(\eta) &= \left(\left(\frac{4}{\hbar}\right)\eta - 2\right)\mathrm{VL}_k^s(\eta) - \mathrm{VL}_{k-1}^s(\eta), \\ k &= 1, 2, \ldots, \end{aligned} \tag{17}$$

where, $\mathrm{VL}_0^s(\eta) = 2, \mathrm{VL}_1^s(\eta) = (4/\hbar)\eta - 2$. It is easy to find that $\mathrm{VL}_k^s(0) = 2(-1)^k, \mathrm{VL}_k^s(\hbar) = 2, k = 0, 1, 2 \ldots$.

The function $\psi(\eta) \in L_2[0, \hbar]$ may be approximated by $\psi_m(\eta)$ as a finite sum with the first $(m + 1)$-terms as follows:

$$\psi_m(\eta) = \sum_{\ell=0}^{m} \zeta_\ell \mathrm{VL}_\ell^s(\eta). \tag{18}$$

Here, we used an approximate formula of $D^{(n)}\psi_m(\eta)$ of the approximated function $\psi_m(\eta)$ defined in form (18), where the authors in [25] derived this formula in the following form:

$$\psi_m^{(n)}(\eta) = \sum_{j=n}^{m}\sum_{p=0}^{j-n}\zeta_j\chi_{j,p,n}\eta^{j-p-n},$$

$$\chi_{j,p,n} = \frac{(-1)^p 4^{j-p}(2j)\Gamma(2j-p)\Gamma(j-p+1)}{\hbar^n\Gamma(p+1)\Gamma(2j-2p+1)\Gamma(j-p+1-n)}. \tag{19}$$

For more details about these polynomials and the convergence analysis of approximations (18) and (19), see [25].

3.2. Procedure Solution Using SCM. We are going to apply the proposed method (SCM) to solve numerically systems (9) and (10). We approximated the unknowns $f(\eta)$ and $\theta(\eta)$ by $f_N(\eta)$ and $\theta_N(\eta)$, respectively, in the following form:

$$\begin{aligned} f_N(\eta) &= \sum_{\ell=0}^{N} a_\ell \mathrm{VL}_\ell^s(\eta), \\ \theta_N(\eta) &= \sum_{\ell=0}^{N} b_\ell \mathrm{VL}_\ell^s(\eta). \end{aligned} \tag{20}$$

By substituting from formula (16) and the formula (15) in equations (9) and (10), we can get the following equations:

$$\begin{aligned} &\left(1+\frac{1}{\beta}\right)\left(\sum_{\ell=3}^{N}\sum_{k=0}^{\ell-3} a_\ell\chi_{\ell,k,3}\eta^{\ell-k-3}\right) + \left(\sum_{\ell=0}^{N} a_\ell \mathrm{VL}_\ell^s(\eta)\right)\left(\sum_{\ell=2}^{N}\sum_{k=0}^{\ell-2} a_\ell\chi_{\ell,k,2}\eta^{\ell-k-2}\right) \\ &-\left(\sum_{\ell=1}^{N}\sum_{k=0}^{\ell-1} a_\ell\chi_{\ell,k,1}\eta^{\ell-k-1}\right)^2 + M^2\left(E_1 - \sum_{\ell=1}^{N}\sum_{k=0}^{\ell-1} a_\ell\chi_{\ell,k,1}\eta^{\ell-k-1}\right) + \Delta\left(\sum_{\ell=0}^{N} b_\ell \mathrm{VL}_\ell^s(\eta)\right) = 0, \end{aligned} \tag{21}$$

$$\begin{aligned} &\left(\frac{1}{\mathrm{Pr}}\right)\left[\left(1+\varepsilon\left(\sum_{\ell=0}^{N} b_\ell \mathrm{VL}_\ell^s(\eta)\right)\right)\left(\sum_{\ell=2}^{N}\sum_{k=0}^{\ell-2} b_\ell\chi_{\ell,k,2}\eta^{\ell-k-2}\right) + \varepsilon\left(\sum_{\ell=1}^{N}\sum_{k=0}^{\ell-1} b_\ell\chi_{\ell,k,1}\eta^{\ell-k-1}\right)^2\right] \\ &+ M^2 Ec\left(\sum_{\ell=1}^{N}\sum_{k=0}^{\ell-1} a_\ell\chi_{\ell,k,1}\eta^{\ell-k-1} - E_1\right)^2 + \left(\sum_{\ell=0}^{N} a_\ell \mathrm{VL}_\ell^s(\eta)\right)\left(\sum_{\ell=1}^{N}\sum_{k=0}^{\ell-1} b_\ell\chi_{\ell,k,1}\eta^{\ell-k-1}\right) \\ &+ Ec\left(1+\frac{1}{\beta}\right)\left(\sum_{\ell=2}^{N}\sum_{k=0}^{\ell-2} a_\ell\chi_{\ell,k,2}\eta^{\ell-k-2}\right)^2 = 0. \end{aligned} \tag{22}$$

We collocate the previous equations (21) and (22) with N of nodes η_p to obtain the following nonlinear system of algebraic equations:

$$\begin{aligned} &\left(1+\frac{1}{\beta}\right)\left(\sum_{\ell=3}^{N}\sum_{k=0}^{\ell-3} a_\ell\chi_{\ell,k,3}\eta_p^{\ell-k-3}\right) + \left(\sum_{\ell=0}^{N} a_\ell \mathrm{VL}_\ell^s(\eta_p)\right)\left(\sum_{\ell=2}^{N}\sum_{k=0}^{\ell-2} a_\ell\chi_{\ell,k,2}\eta_p^{\ell-k-2}\right) \\ &-\left(\sum_{\ell=1}^{N}\sum_{k=0}^{\ell-1} a_\ell\chi_{\ell,k,1}\eta_p^{\ell-k-1}\right)^2 + M^2\left(E_1 - \sum_{\ell=1}^{N}\sum_{k=0}^{\ell-1} a_\ell\chi_{\ell,k,1}\eta_p^{\ell-k-1}\right) + \Delta\left(\sum_{\ell=0}^{N} b_\ell \mathrm{VL}_\ell^s(\eta_p)\right) = 0, \end{aligned} \tag{23}$$

$$\begin{aligned} &\left(\frac{1}{\mathrm{Pr}}\right)\left[\left(1+\varepsilon\left(\sum_{\ell=0}^{N} b_\ell \mathrm{VL}_\ell^s(\eta_p)\right)\right)\left(\sum_{\ell=2}^{N}\sum_{k=0}^{\ell-2} b_\ell\chi_{\ell,k,2}\eta_p^{\ell-k-2}\right) + \varepsilon\left(\sum_{\ell=1}^{N}\sum_{k=0}^{\ell-1} b_\ell\chi_{\ell,k,1}\eta_p^{\ell-k-1}\right)^2\right] \\ &+ M^2 Ec\left(\sum_{\ell=1}^{N}\sum_{k=0}^{\ell-1} a_\ell\chi_{\ell,k,1}\eta_p^{\ell-k-1} - E_1\right)^2 + \left(\sum_{\ell=0}^{N} a_\ell \mathrm{VL}_\ell^s(\eta_p)\right)\left(\sum_{\ell=1}^{N}\sum_{k=0}^{\ell-1} b_\ell\chi_{\ell,k,1}\eta_p^{\ell-k-1}\right) \\ &+ Ec\left(1+\frac{1}{\beta}\right)\left(\sum_{\ell=2}^{N}\sum_{k=0}^{\ell-2} a_\ell\chi_{\ell,k,2}\eta_p^{\ell-k-2}\right)^2 = 0. \end{aligned} \tag{24}$$

We substituted from equation (20) in the boundary conditions (11) and (12) to expressed in the following equations:

$$\begin{aligned}
\sum_{\ell=0}^{N} 2(-1)^{\ell} a_{\ell} &= 0,\\
\sum_{\ell=0}^{N} a_{\ell}\left(\mathrm{VL}_{\ell}^{s'}(0) - \lambda\left(1+\frac{1}{\beta}\right)\mathrm{VL}_{\ell}^{s''}(0)\right) &= 1,\\
\sum_{\ell=0}^{N}\left(2(-1)^{\ell} - S_T \mathrm{VL}_{\ell}^{s'}(0)\right) b_{\ell} &= 1,
\end{aligned} \tag{25}$$

$$\begin{aligned}
\sum_{\ell=0}^{N} a_{\ell} \mathrm{VL}_{\ell}^{s'}(\hbar) &= 0,\\
\sum_{\ell=0}^{N} 2b_{\ell} &= 0.
\end{aligned} \tag{26}$$

Equations (23)–(26) construct a system of $2(N+1)$ algebraic equations. Then, we used the Newton iteration method to solve this system for the unknowns a_{ℓ}, b_{ℓ}, where $\ell = 0, 1, \ldots, N$, to obtain the approximate solution.

4. Code Verification

By completing the particular validations shown in Table 1, this section checks the technical correctness of the completed numerical code. For the case of Newtonian fluid $\beta \longrightarrow \infty$, Table 1 compares the numerical values of $-f''(0)$ that were reported by Hasnain et al. [26] for various values of M^2 when $E_1 = \Delta = \lambda = 0$. The findings are seen to be in very good agreement with the published studies. Therefore, Table 1 ensures that the current numerical solutions are validated against earlier literature.

5. Main Results

The following figures and table describe many pertinent parameters related to dimensionless velocity, dimensionless temperature, local Nusselt number, and skin friction coefficient. Firstly, the range of the parameters that govern our model can be mentioned as $0.0 \le M \le 0.8, 0.0 \le E_1 \le 1.0, 0.0 \le \Delta \le 0.5, 0.5 \le \beta \le 0.5, 0.0 \le \lambda \le 0.3, 0.0 \le \varepsilon \le 0.6$ and $0.0 \le Ec \le 0.6$. Therefore, the fixed values for the same controlling parameters can be employed through the graphical illustrations: $M = 0.2, E_1 = 0.5, \Delta = 0.2, \beta = 0.5, \lambda = 0.1, \varepsilon = 0.2$, and $Ec = 0.5$. The fluid velocity is considerably suppressed when subjected to an increased magnetic number, as seen in Figure 2(a). In actuality, a stronger magnetic field produces more drag force, which slows down the movement of the fluid. Therefore, it is projected that this drag force will have an enhanced effect on the thermal field at high magnetic number values as noted in Figure 2(b). Physically, adding a magnetic field increases magnetic irreversibility; however, Lorentz forces reduce fluid flow velocity and increase fluid temperature.

Figures 3(a) and 3(b) showed how the local electric parameter E_1 affected the profiles of velocity and temperature. The increasing value of the local parameter in these graphs demonstrates an increase in the momentum and temperature fields of the Casson fluid. As a result, at higher values of the local electric parameter, the boundary layer (BL) thickness increases. Physically, the presence of an electric field may provide an induction force for the fluid particles, causing the fluid flow motion within the boundary layer to increase.

The effects of the mixed convection parameter Δ on the momentum field and the thermal field are presented in Figure 4 for different quantities of the parameter. Figure 4(a) shows that at higher values of Δ, the velocity curves are of a rising nature through the BL region. Furthermore, the thermal field is slightly diminished by the same parameter Δ as observed from Figure 4(b). Physically, there is an increase in fluid velocity and a minor reduction of the temperature distribution due to the strong mixed convection parameter, which works as a pressure gradient and dominates over the resistance.

Figure 5 shows, respectively, how $f'(\eta)$ and $\theta(\eta)$ fields are affected by the Casson parameter β. Physically, the Casson fluid behaves more similar to a Newtonian fluid when the values of β are increased. Therefore, increasing β results in a declining phenomenon in $f'(\eta)$ and $\theta(\eta)$.

Figure 6 shows the characteristics of $\theta(\eta)$ and $f'(\eta)$ under the impact of the slip velocity parameter λ. Clearly, greater resistive forces via the fluid layers are produced by slip velocity parameter λ with bigger values, which reduce fluid velocity and marginally raise the temperature. Physically, it is obvious that as the slip velocity impact rises, the fluid flow becomes more impeded, limiting the thickness of the boundary layer and the temperature distribution.

Figures 7(a) and 7(b), respectively, show the thermal field's behaviors for the ranges of the thermal conductivity parameter ε, and the Eckert number Ec were taken into consideration. This analysis shows that increasing the values of Ec and ε improves the temperature distribution. Additionally, the thickness of the thermal BL increases as the same parameters are gradually improved. Physically, an increase in the Eckert number increases the thermal system's kinetic energy. As a result, the thermal field grew. Also, the fluid receives thermal energy from the thermal conductivity characteristic. More thermal energy will travel through the fluid when this value rises.

The curves in Figure 8 show how temperature profiles have changed over time about changes in the Prandtl Pr and thermal slip S_T parameters. Figure 8(a) shows temperature profiles for three different values of Pr ($\mathrm{Pr} = 1.0, \mathrm{Pr} = 2.0, \mathrm{Pr} = 3.0,$) at ($S_T = 1.0$), while Figure 8(b) shows temperature profiles about the thermal slip parameter S_T at $\mathrm{Pr} = 2.0$. This graphical illustration shows that both parameters show a discernible diminishing in the sheet temperature $\theta(0)$ and for the temperature profiles $\theta(\eta)$. Physically, these observations are made because the thermal properties between the heating fluid and the solid surface are greatly weakened by the advanced values of the Prandtl and thermal slip parameters.

Table 1: Comparison of $-f''(0)$ with the results of Hasnain et al. [26] when $E_1 = \Delta = \lambda = 0$ and $\beta \longrightarrow \infty$.

M^2	Hasnain et al. [26]	Present work
0.0	1.000	1.000000000
0.2	1.095	1.095101208
0.5	1.224	1.223999820
1.0	1.414	1.414104019
1.2	1.483	1.482998590
1.5	1.581	1.581205891
2.0	1.732	1.732015980

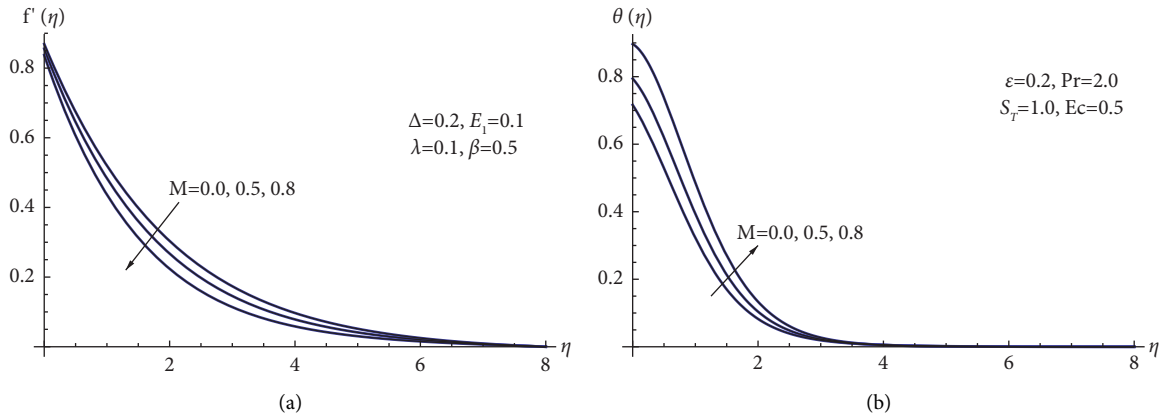

Figure 2: (a) $f'(\eta)$ versus M. (b) $\theta(\eta)$ for picked M.

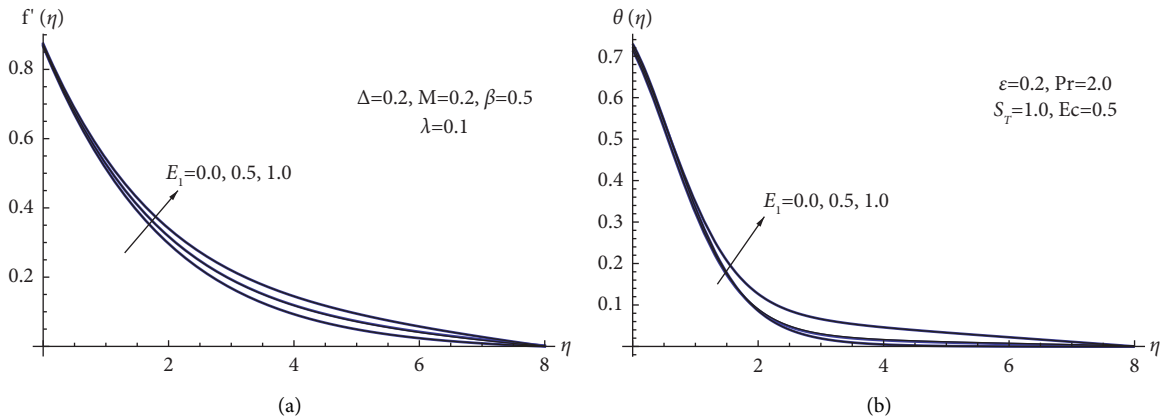

Figure 3: (a) $f'(\eta)$ versus E_1. (b) $\theta(\eta)$ for picked E_1.

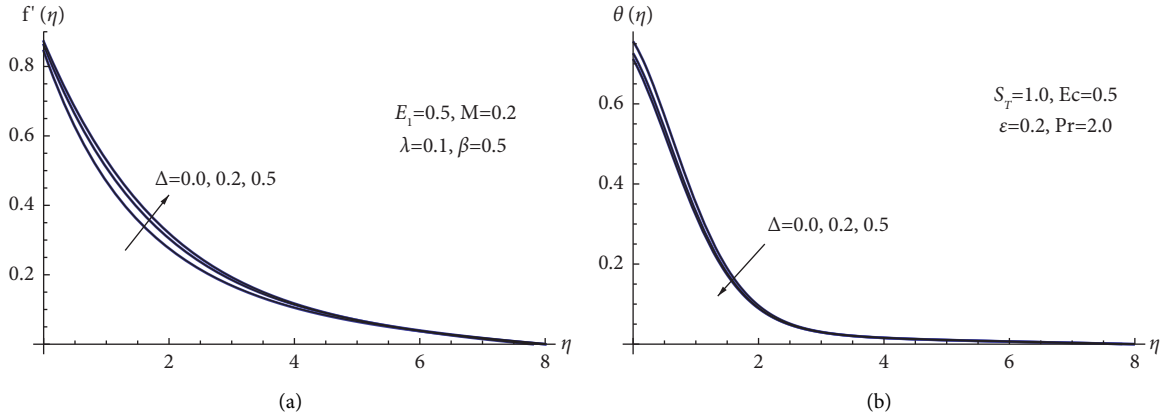

Figure 4: (a) $f'(\eta)$ versus Δ. (b) $\theta(\eta)$ for picked Δ.

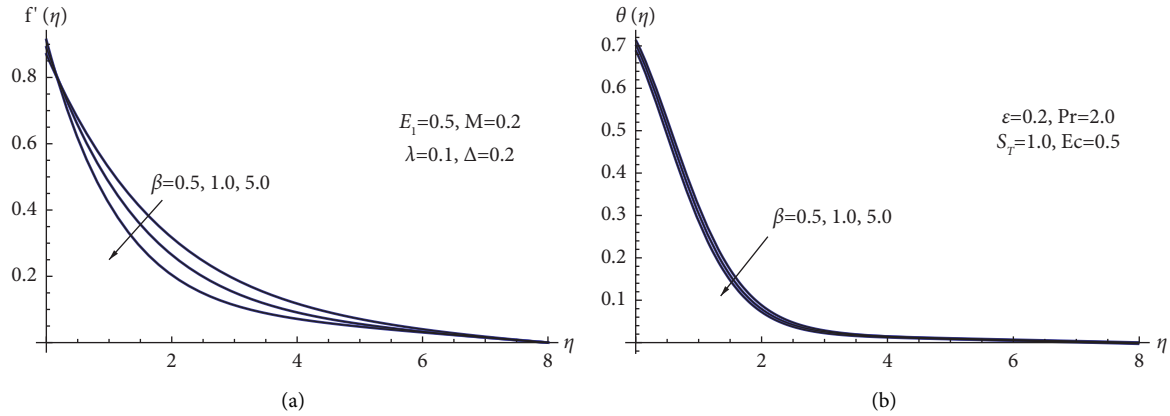

Figure 5: (a) $f^{'}(\eta)$ versus β. (b) $\theta(\eta)$ for picked β.

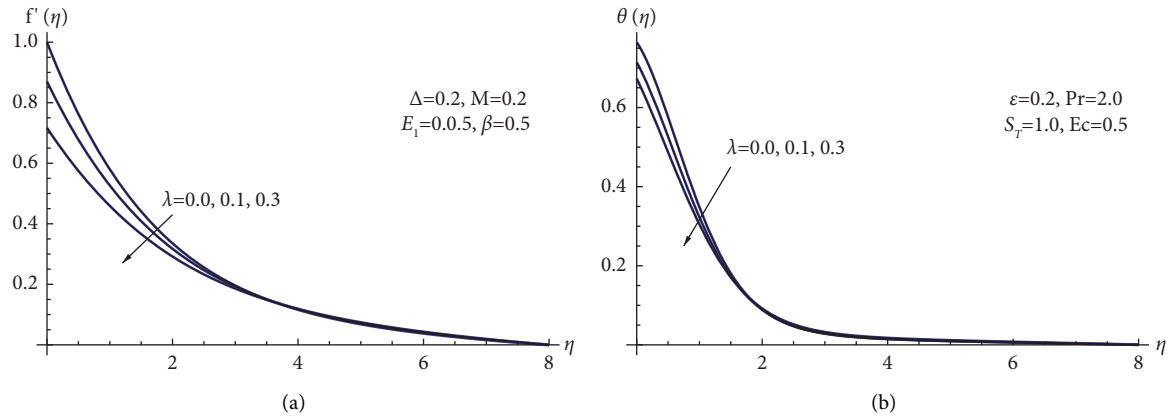

Figure 6: (a) $f^{'}(\eta)$ versus λ. (b) $\theta(\eta)$ for picked λ.

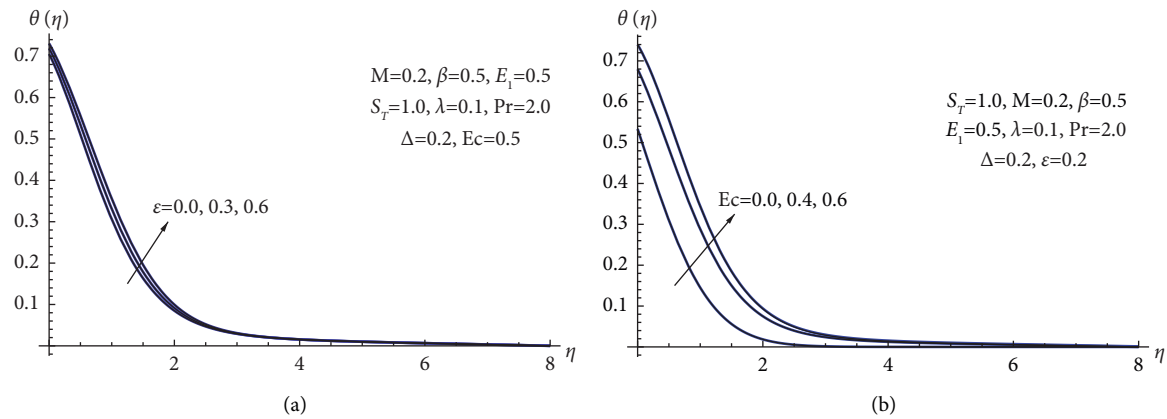

Figure 7: (a) $\theta(\eta)$ versus ε. (b) $\theta(\eta)$ for picked Ec.

To observe the behavior of parameters affecting the local Nusselt number $Nu_x Re_x^{-1/2}$ and the skin friction coefficient $C_f Re_x^{1/2}$, Table 2 is now generated. This table makes it abundantly clear that the $C_f Re_x^{1/2}$ and the $Nu_x Re_x^{-1/2}$ have inverse relationships with the magnetic number. The local Nusselt number $Nu_x Re_x^{-1/2}$ decreases as both the thermal slip parameter and the magnetic number rises, yet the $C_f Re_x^{1/2}$ upsurges. Additionally, the $Nu_x Re_x^{-1/2}$ rises together with the value of the thermal conductivity parameter, whereas the $C_f Re_x^{1/2}$ declines. The skin friction coefficient $C_f Re_x^{1/2}$ also decreases when the Eckert number rises, as does the $Nu_x Re_x^{-1/2}$, whereas the reverse trend is noted for the Prandtl number. Additionally, the $C_f Re_x^{1/2}$ decreases, but the local Nusselt number increases when the local electric, mixed convection, Casson, and slip velocity parameters are improved.

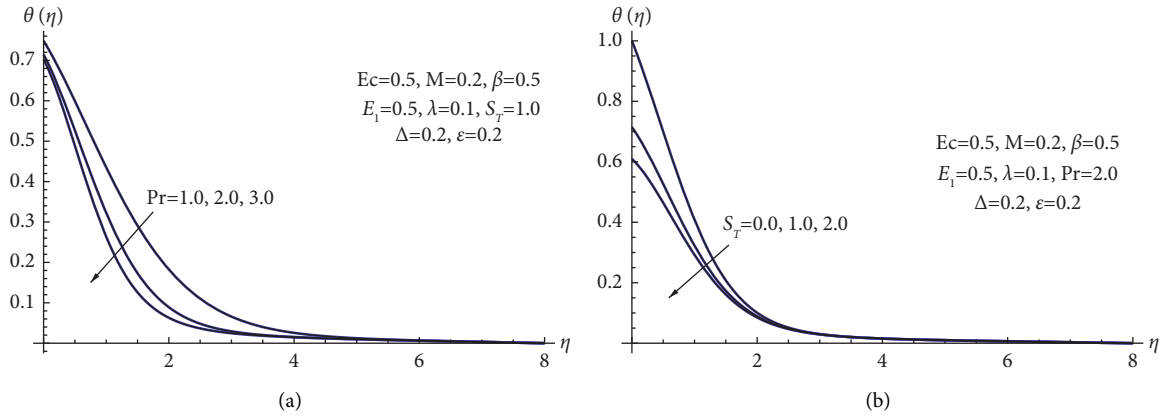

FIGURE 8: (a) $\theta(\eta)$ versus Pr. (b) $\theta(\eta)$ for picked S_T.

TABLE 2: Values for $C_f Re_x^{1/2}$ and $Nu_x Re_x^{-1/2}$ for different quantities of M, E_1, Δ, β, Pr, S_T, λ, ε, and Ec.

M	E_1	Δ	β	λ	ε	Ec	Pr	S_T	$C_f Re_x^{1/2}$	$Nu_x Re_x^{-1/2}$
0.0	0.1	0.2	0.5	0.1	0.2	0.5	2.0	1.0	1.309561	0.340459
0.5	0.1	0.2	0.5	0.1	0.2	0.5	2.0	1.0	1.443031	0.246962
0.8	0.1	0.2	0.5	0.1	0.2	0.5	2.0	1.0	1.624750	0.124142
0.2	0.0	0.2	0.5	0.1	0.2	0.5	2.0	1.0	1.332701	0.324096
0.2	0.5	0.2	0.5	0.1	0.2	0.5	2.0	1.0	1.298980	0.343232
0.2	1.0	0.2	0.5	0.1	0.2	0.5	2.0	1.0	1.258032	0.353212
0.2	0.5	0.0	0.5	0.1	0.2	0.5	2.0	1.0	1.551961	0.292947
0.2	0.5	0.2	0.5	0.1	0.2	0.5	2.0	1.0	1.298980	0.343232
0.2	0.5	0.5	0.5	0.1	0.2	0.5	2.0	1.0	1.280811	0.365372
0.2	0.5	0.2	0.5	0.1	0.2	0.5	2.0	1.0	1.298980	0.343232
0.2	0.5	0.2	1.0	0.1	0.2	0.5	2.0	1.0	1.089781	0.356141
0.2	0.5	0.2	5.0	0.1	0.2	0.5	2.0	1.0	0.866855	0.372145
0.2	0.5	0.2	0.5	0.0	0.2	0.5	2.0	1.0	1.623691	0.281660
0.2	0.5	0.2	0.5	0.1	0.2	0.5	2.0	1.0	1.299251	0.342753
0.2	0.5	0.2	0.5	0.3	0.2	0.5	2.0	1.0	0.943656	0.392202
0.2	0.5	0.2	0.5	0.1	0.0	0.5	2.0	1.0	1.301760	0.294773
0.2	0.5	0.2	0.5	0.1	0.3	0.5	2.0	1.0	1.298121	0.365601
0.2	0.5	0.2	0.5	0.1	0.6	0.5	2.0	1.0	1.290153	0.430821
0.2	0.5	0.2	0.5	0.1	0.2	0.0	2.0	1.0	1.334372	0.559788
0.2	0.5	0.2	0.5	0.1	0.2	0.4	2.0	1.0	1.306120	0.384397
0.2	0.5	0.2	0.5	0.1	0.2	0.6	2.0	1.0	1.283943	0.312069
0.2	0.5	0.2	0.5	0.1	0.2	0.5	1.0	1.0	1.280372	0.302028
0.2	0.5	0.2	0.5	0.1	0.2	0.5	2.0	1.0	1.298980	0.343232
0.2	0.5	0.2	0.5	0.1	0.2	0.5	3.0	1.0	1.306984	0.356784
0.2	0.5	0.2	0.5	0.1	0.2	0.5	2.0	0.0	1.274874	0.626389
0.2	0.5	0.2	0.5	0.1	0.2	0.5	2.0	1.0	1.298980	0.343232
0.2	0.5	0.2	0.5	0.1	0.2	0.5	2.0	2.0	1.308183	0.234157

6. Conclusions

Under the impacts of Ohmic dissipation and the slip velocity conditions, the mixed convection flow of non-Newtonian Casson fluid is studied numerically. To compute and outline the changing reactions of flow velocities and temperature when the physical parameters are altered in their proper ranges, SCM based on the shifted VLPs is introduced as a numeric technique. The important results are listed below:

(1) The local electric parameter causes a rise in local temperature and the Nusselt number.

(2) Increasing the Ec values causes a decrease in the local Nusselt number and skin friction coefficient.

(3) The heat transfer rate increases while the local skin friction reduces for high Casson and mixed convection parameter values.

(4) By raising the value of the slip velocity parameter, the temperature distribution is enhanced with slight changes in thermal boundary layer thickness.

(5) The presence of M enhances the local skin friction coefficient, but it also limits fluid flow and raises the fluid temperature.

(6) In contrast to Δ and β, the temperature marginally drops across the boundary layer.

(7) Since the modified Darcy law is more appropriate for the non-Newtonian fluid flow within the porous medium, therefore, in the future, this work can be expanded by taking into consideration the impact of thermal slip and the variable heat flux on the flow behavior through a porous medium that is constrained by the modified Darcy law.

Nomenclature

a: Constant (s^{-1})
B_0: Magnetic field strength (T)
c_p: Specific heat ($Jkg^{-1}K^{-1}$)
C_f: Skin friction coefficient
E_0: Electric field (Vm^{-1})
E_1: Local electric parameter
Ec: Eckert number
g: Gravitational acceleration (ms^{-2})
f: Dimensionless stream function
K: Thermal slip coefficient (m)
M: Magnetic parameter
Nu_x: Local Nusselt number
Pr: Prandtl number
Re_x: Local reynolds number
S_T: Thermal slip parameter
T: Temperature of the fluid (K)
T_w: Sheet temperature (K)

T_∞: Temperature away the sheet (K)
u, v: $x-$ and $y-$ direction of the fluid velocity (ms^{-1})
U_w: Sheet velocity (ms^{-1})
x, y: Cartesian coordinates (m)

Greek Symbols
β: Casson parameter
μ: Fluid viscosity ($kgm^{-1}s^{-1}$)
κ: Thermal conductivity ($Wm^{-1}K^{-1}$)
κ_∞: Ambient fluid thermal conductivity ($Wm^{-1}K^{-1}$)
η: Similarity variable
θ: Nondimensional temperature
ν: Kinematic viscosity (m^2s^{-1})
ε: Thermal conductivity parameter
δ: Coefficient of thermal expansion (K^{-1})
Δ: Mixed convection parameter
ρ: Fluid density (kgm^{-3})
λ: Slip velocity parameter
λ_1: Slip velocity factor (m)
σ: Electrical conductivity (Vm^{-1})

Superscripts
$'$: Differentiation with respect to η
∞: Free stream condition
w: Wall condition.

Data Availability

No data were used to support this study.

Conflicts of Interest

The authors declare that they have no conflicts of interest.

Authors' Contributions

All authors contributed equally and significantly in writing this article. All authors read and approved the final manuscript.

Acknowledgments

The authors extend their appreciation to the Deanship of Scientific Research at Imam Mohammad Ibn Saud Islamic University for funding this work through Research Group no. RG-21-09-42.

References

[1] J. Mudassar, S. Asghar, and M. Muhammad, "Analytical solutions of the boundary layer flow of power-law fluid over a power-law stretching surface," *Communications in Nonlinear Science and Numerical Simulation*, vol. 18, pp. 1143–1150, 2013.

[2] G. S. Seth, A. Bhattacharyya, and M. K. Mishra, "Study of partial slip mechanism on free convection flow of viscoelastic fluid past a nonlinear stretching surface," *Computational Thermal Sciences: International Journal*, vol. 11, pp. 105–117, 2019.

[3] T. Hayat, S. Asad, M. Mustafa, and A. Alsaedi, "Boundary layer flow of Carreau fluid over a convectively heated stretching sheet," *Applied Mathematics and Computation*, vol. 246, pp. 12–22, 2014.

[4] K. Hosseinzadeh, M. Gholinia, B. Jafari, A. Ghanbarpour, H. Olfian, and D. D. Ganji, "Nonlinear thermal radiation and chemical reaction effects on Maxwell fluid flow with convectively heated plate in a porous medium," *Heat Transfer - Asian Research*, vol. 48, no. 2, pp. 744–759, 2019.

[5] P. P. Humane, V. S. Patil, and A. B. Patil, "Chemical reaction and thermal radiation effects on magnetohydrodynamics flow of Casson–Williamson nanofluid over a porous stretching surface," *Proceedings of the Institution of Mechanical Engineers - Part E: Journal of Process Mechanical Engineering*, vol. 235, no. 6, pp. 2008–2018, 2021.

[6] K. Singh and M. Kumar, "The effect of chemical reaction and double stratification on MHD free convection in a micropolar fluid with heat generation and Ohmic heating," *Jordan Journal of Mechanical and Industrial Engineering*, vol. 9, pp. 279–288, 2015.

[7] K. Singh, A. K. Pandey, and M. Kumar, "Analytical approach to a stagnation point flow and heat transfer of a micropolar fluid via a permeable shrinking sheet with slip and convective boundary conditions," *Heat Transfer Research*, vol. 50, no. 8, pp. 739–756, 2019.

[8] T. Hayat, I. Ullah, A. Alsaedi, and M. Farooq, "MHD flow of Powell-Eyring nanofluid over a non-linear stretching sheet with variable thickness," *Results in Physics*, vol. 7, pp. 189–196, 2017.

[9] M. Patel, D. C. Levin, L. Parker, and V. M. Rao, "Laminar boundary flow of sisko fluid," *Journal of the American College of Radiology: JACR*, vol. 12, no. 9, pp. 909–914, 2015.

[10] M. Tamoor, M. Waqas, M. I. Khan, A. Alsaedi, and T. Hayat, "Magnetohydrodynamic flow of Casson fluid over a stretching cylinder," *Results in Physics*, vol. 7, pp. 498–502, 2017.

[11] M. Mustafa, T. Hayat, P. Ioan, and A. Hendi, "Stagnation-point flow and heat transfer of a Casson fluid towards a stretching sheet," *Zeitschrift für Naturforschung A*, vol. 67, no. 1-2, pp. 70–76, 2012.

[12] S. Mukhopadhyay, P. R. De, K. Bhattacharyya, and G. C. Layek, "Casson fluid flow over an unsteady stretching surface," *Ain Shams Engineering Journal*, vol. 4, pp. 933–938, 2013.

[13] H. Upreti, A. K. Pandey, Z. Uddin, and M. Kumar, "Thermophoresis and Brownian motion effects on 3D flow of Casson nanofluid consisting microorganisms over a Riga plate using PSO: a numerical study," *Chinese Journal of Physics*, vol. 78, pp. 234–270, 2022.

[14] W. M. Abd-Elhameed and Y. H. Youssri, "Connection formulae between generalized Lucas polynomials and some Jacobi polynomials: application to certain types of fourth-order BVPs," *International Journal of Algorithms, Computing and Mathematics*, vol. 6, no. 2, pp. 45–19, 2020.

[15] M. M. Khader and M. Adel, "Numerical and theoretical treatment based on the compact finite difference and spectral collocation algorithms of the space fractional-order Fisher's equation," *International Journal of Modern Physics C*, vol. 31, no. 9, Article ID 2050122, 2020.

[16] Ö. Oruç, "A new algorithm based on Lucas polynomials for approximate solution of 1D and 2D nonlinear generalized Benjamin-Bona-Mahony-Burgers equation," *Computers & Mathematics with Applications*, vol. 74, no. 12, pp. 3042–3057, 2017.

[17] Ö. Oruç, "A new numerical treatment based on Lucas polynomials for 1D and 2D sinh-Gordon equation," *Communications in Nonlinear Science and Numerical Simulation*, vol. 57, pp. 14–25, 2018.

[18] T. Hayat, A. Shafiq, and A. Alsaedi, "Hydromagnetic boundary layer flow of Williamson fluid in the presence of thermal radiation and Ohmic dissipation," *Alexandria Engineering Journal*, vol. 55, no. 3, Article ID 552229, 2016.

[19] A. M. Megahed, "Heat flux and variable thermal conductivity effects on Casson flow and heat transfer due to an exponentially stretching sheet with viscous dissipation and heat generation," *International Journal of Chemical Reactor Engineering*, vol. 14, no. 1, pp. 167–174, 2016.

[20] A. A. Afify, "The influence of slip boundary condition on Casson nanofluid flow over a stretching sheet in the presence of viscous dissipation and chemical reaction," *Mathematical Problems in Engineering*, vol. 2017, Article ID 3804751, 12 pages, 2017.

[21] M. A. A. Mahmoud, "The effects of variable fluid properties on MHD Maxwell fluids over a stretching surface in the presence of heat generation/absorption," *Chemical Engineering Communications*, vol. 198, no. 1, pp. 131–146, 2010.

[22] M. A. Rahman, M. J. Uddin, O. A. Bég, and A. Kadir, "Influence of variable viscosity and thermal conductivity, hydrodynamic, and thermal slips on magnetohydrodynamic micropolar flow: a numerical study," *Heat Transfer - Asian Research*, vol. 48, no. 8, pp. 3928–3944, 2019.

[23] A. F. Horadam, *Vieta Polynomials*, The University of New England, Armidaie, Australia, 2000.

[24] P. Agarwal and A. A. El-Sayed, "Vieta-Lucas polynomials for solving a fractional-order mathematical physics model," *Advances in Difference Equations*, vol. 2020, pp. 626–718, 2020.

[25] M. Z. Youssef, M. M. Khader, I. Al-Dayel, and W. E. Ahmed, "Solving fractional generalized Fisher–Kolmogorov–Petrovsky–Piskunov's equation using compact-finite different methods together with spectral collocation algorithms," *Journal of Mathematics*, vol. 2022, Article ID 1901131, 9 pages, 2022.

[26] J. Hasnain, Z. Abbas, M. Sheikh, and S. Aly, "Analysis of dusty Casson fluid flow past a permeable stretching sheet bearing power law temperature and magnetic field," *International Journal of Numerical Methods for Heat and Fluid Flow*, vol. 30, no. 6, pp. 3463–3480, 2020.